Journal of the Australian Ceramic Society
https://doi.org/10.1007/s41779-019-00336-4

RESEARCH

Effect of lanthanum oxide additive on the sinterability, physical/mechanical, and bioactivity properties of hydroxyapatite-alpha alumina composite

Serdar Pazarlioglu [1] · Serdar Salman [2]

Received: 25 July 2018 / Accepted: 5 March 2019
© Australian Ceramic Society 2019

Abstract
The aim of this study was to evaluate the effect of lanthanum oxide (La_2O_3) additive on the microstructural, physical, mechanical, and in vitro bioactivity properties of hydroxyapatite (HA)-alpha alumina (α-Al_2O_3) composite. The monolithic HA as well as composites of HA-5 wt% α-Al_2O_3 and HA-5 wt% Al_2O_3-(0.5 wt%, 1.5 wt%, and 2.5 wt%) La_2O_3 were uniaxially pelleted at 350 MPa with a size of ∅11 and 11 mm^2 and sintered at the temperatures ranging from 1100 to 1300 °C for 4 h. The highest mechanical strength values of 130.20 ± 6.22 MPa, 60.27 ± 9.93 MPa, and 0.96 ± 0.05 MPa $m^{1/2}$ for compressive strength ($\sigma_{compressive}$), three-point bending strength ($\sigma_{three\text{-}point\ bending}$), and fracture toughness (K_{ic}) were obtained for monolithic HA, respectively. While the decomposition (transformation of HA to secondary phases such as beta-tricalcium phosphate (β-TCP), alpha-tricalcium phosphate (α-TCP), and calcium oxide (CaO)) ratio was about 5.7% for monolithic HA, it attained to 27.4% for HA-5wt% α-Al_2O_3 composite. However, addition of La_2O_3 to HA-5 wt% α-Al_2O_3 composite contributed to decreasing of decomposition from 27.4 to 22.0%. The mechanical strength values of $\sigma_{compressive}$ of 214 ± 32.50 MPa, $\sigma_{three\text{-}point\ bending}$ of 75.70 ± 2.40 MPa, and K_{ic} of 1.95 ± 0.10 MPa $m^{1/2}$ were obtained for HA-5wt% α-Al_2O_3 composite. SEM images exhibited that α-Al_2O_3 led to decreasing the in vitro bioactivity of HA. However, La_2O_3 additive contributed to improvement of the mechanical as well as bioactivity properties of HA-5 wt% α-Al_2O_3 composite. HA-5 wt% α-Al_2O_3-0.5 wt% La_2O_3 composite can be used as a bioceramic in human body, because it has enough mechanical properties as well as its desirable in vitro bioactivity.

Keywords Hydroxyapatite · Alpha-alumina · Lanthanum oxide · Sintering

Introduction

Surplus demands and requirements for synthetic bone substitutes have been experienced in the last few decades, owing to the number of accidents/trauma and inherent bone defects by birth/age/diseases [1]. Implantation of bone autografts or allografts is the strategy in healing large bone defects. However, there are some drawbacks on this strategy, which limit their widespread usage, such as extended surgical time and donor site morbidity for autograft, and adverse immune response and pathogen disease transmission for allograft. These problems have guided researchers for the development of bone substitute materials [2]. Some ceramic materials such as zirconium oxide (ZrO_2), alumina (Al_2O_3), and hydroxyapatite (HA) have become attractive materials for the repair of damaged hard tissues of the human body. Among these ceramic materials, particular attention has been given to HA due to it has the same chemical composition with mineral part of bone. The ability of HA to form bioactive fixation with the surrounding bone tissues is also well known. However, dense HA not only has high brittleness but also has low fracture toughness which hardly exceeds 1 MPa $m^{1/2}$. Because of its low mechanical properties, implantation of this material is restricted to unstressed regions of the body [3]. Since the mechanical properties of HA is limited, the incorporation of resistant oxide phase such as zirconia (ZrO_2) [4], silica (SiO_2) [5], titania (TiO_2) [6], and yttria (Y_2O_3) [7] has been proposed to

✉ Serdar Pazarlioglu
spazarlioglu@marmara.edu.tr

[1] Technology Faculty, Materials Science and Engineering Department, Marmara University, Goztepe Campus, 34722 Istanbul, Turkey

[2] National Defence University, Besiktas Campus, 34334 Istanbul, Turkey

Published online: 27 March 2019

optimize biocompatibility and enhance the mechanical properties.

Alpha-alumina (α-Al_2O_3) has been widely investigated as a reinforcing agent for HA due to its cost-effective and well-accessible option for enhancing HA properties, especially the mechanical properties [8]. Eskandari et al. [9] reported that the addition of α-Al_2O_3 into HA might increase the flexural strength up to 85.8 MPa as well as the Vickers microhardness which can be around 5.12 GPa. As reported by Balani et al. [10], mixing of about 20 wt% α-Al_2O_3 into HA showed hardness and toughness of 5.9 GPa and 0.45 MPa $m^{1/2}$, respectively. Li et al. [11] stated that the flexural strength of HA/(30–85 vol%)α-Al_2O_3 composite decreased from 700 to 150 MPa depending on HA ratio. But the addition of α-Al_2O_3 from 10 to 30% alters the phase composition and morphological distribution of HA, and the rise in sintering temperature and increase in weight percent of α-Al_2O_3 content also facilitates the decomposition of HA into secondary phases such as beta-tricalcium phosphate (β-TCP), alpha-tricalcium phosphate (α-TCP), and calcium oxide (CaO) [12, 13]. To eliminate these problems, Al_2O_3 should be added at low loading to HA. Another approach is the addition of a dopant material to inhibit the decomposition of HA in HA-Al_2O_3 composites [14]. For the second approach, numerous studies have been performed to investigate the effect of additives, such as magnesium fluoride (MgF_2) [15], calcium fluoride (CaF_2) [16], commercially inert glass (CIG) [17], clinoptilolite [18], bioglass [19], tricalcium phosphate [20], and titania [21] on the sinterability and physical and/or mechanical properties of HA-Al_2O_3 binary composites. As reported by Park et al. [15], in the case of MgF_2 addition at the amount of 5 vol%, a relatively high mechanical property (flexural strength 170 MPa; Vickers hardness 7 GPa) was obtained compared to monolithic HA (flexural strength 70 MPa; Vickers hardness 2 GPa). Kim et al. [16] found that addition of 5 vol% CaF_2 (four-point flexural strength 125 MPa; Vickers hardness 8 GPa; elastic modulus 135 GPa; fracture toughness 1.2 MPa $m^{-1/2}$) contributed to mechanical properties of HA-20 vol%Al_2O_3 composite (four-point flexural strength 50 MPa; Vickers hardness 4 GPa; elastic modulus 115 GPa; fracture toughness 0.65 MPa $m^{-1/2}$). Bulut et al. [17] investigated the effect of CIG additive (at amount of 5 wt% and 10 wt%, respectively) to HA-10 wt% Al_2O_3 composite. They found that the high mechanical strength values were obtained for 10 wt% CIG added samples (Vickers hardness 129; compressive strength 53 MPa). Kalkandelen et al. [17] studied on the (5 wt%, 10 wt%, and 15 wt%) clinoptilolite-(5 wt%, 10 wt%, and 15 wt%) alumina-bovine hydroxyapatite composites. They reported that the highest mechanical strengths were obtained to 15 wt% clinoptilolite-15 wt% alumina-bovine hydroxyapatite composites, after sintering at 1300 °C. (density 2.337 ± 0.018 g/cm^3; Vickers hardness 305 ± 56.0; compressive strength 105.6 ± 15.2; elastic modulus 1275 ± 112 MPa). Wang et al. [19] indicated that a large number of HA particles stacked together are subjected to form roughened surface, wherein microcracks, voids, and pores had observed, suggesting that pressureless sintering was not the best way for densification of HA-bioglass-Al_2O_3 composite. Yilmaz et al. [20] studied on the porosity levels of 10–50 wt% Al_2O_3-(10 wt%) bovine hydroxyapatite-(80–40 wt%) tricalcium phosphate (TCP) composites. They found that the composites of α-Al_2O_3-HA-TCP included the 38–44% apparent porosity after sintering between 500 and 1300 °C for 2 h. Chaari et al. [21] investigated the mechanical properties of alumina-fluorapatite composites with different titania additive amounts (0, 0.5, 1, 1.4, 2, 3, 4, and 5 wt%) between 1200 and 1600 °C. The optimum values of densification and mechanical properties of composites reached with 1.4 wt% of titania after the sintering process at 1500 °C for 1 h. Thus, the rupture strength of alumina-26.52 wt% FAp-1.4 wt% TiO_2 reaches 75 MPa. At higher temperature and beyond 1.4 wt% TiO_2, the densification and mechanical properties were hindered by the formation of both intergranular porosity and secondary phase.

Lanthanum oxide (La_2O_3) is another oxide ceramic that can be used for improving properties of HA. It has been reported by Branda et al. [22] that the low rate of La_2O_3 (up to 0.6% by weight) does not adversely affect the bioactivity property of the CaO-SiO_2 bioglass. As indicated by Shin-Ike et al. [23], the tensile and three-point bending strengths of HA might be improved by La_2O_3 addition. HA-La_2O_3 composites do not cause a reaction that is adversely affecting the immune system in the in vivo environment [24]. It was also reported by Bozkurt et al. [25] that the addition of La_2O_3 at about 2.5 wt% contributed to improvement of the mechanical strength of HA. In addition to these studies, the effect of La_2O_3 additive to HA-ZrO_2 [26] and to HA-B_2O_3 [27] binary composites was also studied. To the best of our knowledge, no study yet has been reported for the cosubstitution of Al_2O_3 and La_2O_3. La_2O_3 additive in the present study was intentionally selected due to its excellent properties such as improving the compressive and three-point bending strength without negative effect on bioactivity of HA, in the light of literature review.

In this study, the microstructural, physical, and mechanical properties of HA-(5 wt%)Al_2O_3 with and without (0 .5wt%, 1 .5wt%, and 2.5 wt%) La_2O_3 were investigated. Moreover, in vitro bioactivity of doped HA was also evaluated.

Materials and methods

Material fabrication

As starting materials, HA (CAS number 1306-06-5; commercial purity, Across Organics Co., Belgium) and α-Al_2O_3 (CAS number 1344-28-1; 99.5% purity, Sigma-Aldrich, USA)

powders were used to fabricate HA-5 wt% α-Al_2O_3 composite. La_2O_3 (CAS number 1312-81-8; ≥ 99.9% purity, Sigma-Aldrich Co., USA) powder at amounts of 0.5 wt%, 1.5 wt%, and 2.5 wt% were added to HA-5 wt% α-Al_2O_3. The abbreviations, description, and the composition of the samples are shown in Table 1. The powders were mixed using a conventional ball milling at 180 rpm for 2 h to obtain the composites of HA-5A, HA-5A-0.5L, HA-5A-1.5L, and HA-5A-2.5L composites. After pelletizing with the dimensions of 11 mm in diameter and 11 mm in height at a pressure load of 350 MPa, mixed powders were sintered in air at 1100 °C, 1200 °C, and 1300 °C at a ramp rate of 5 °C min^{-1} and soaking time of 4 h and then cooled to room temperature at a ramp rate of 5 °C min^{-1} at air atmosphere.

Characterization and mechanical test

Phase analysis using a Philips X'Pert X-ray diffraction (XRD, Netherlands) device was performed with Cu-Kα (λ = 1.5406 Å) as the radiation source at a scan speed of 0.6°min^{-1} and a step scan of 0.02° in the range of 2θ values between 10° and 80°. To determine the decomposition of HA (JCPDS card number of 98-008-0526) into β and/or α-TCP (β-TCP; JCPDS card number 98-007-6896, α-TCP; JCPDS card number 98-007-8499), Rietveld analysis was used. The surface morphology of the sintered samples was determined using FEI Sirion XL30 scanning electron microscope (SEM, USA) after gold sputtering. The variations in the average grain size were determined by the lineal intercept method [28]. The relative density of the sintered samples was determined by Archimedean method. The theoretical density of the composites was calculated from the known weights, *W*, and densities, *ρ*, by the following formula:

$$\rho_t = \frac{w_A + w_B + w_C}{\frac{w_A}{\rho_A} + \frac{w_B}{\rho_B} + \frac{w_c}{\rho_C}} \quad (1)$$

where ρ_t is the theoretical density of the composites. w_A, w_B, and w_C are the weight ratios of HA, Al_2O_3, and La_2O_3 in the composites. ρ_A, ρ_B, and ρ_C are the theoretical densities of HA (3.156 g/cm^3 [29]), Al_2O_3 (3.970 g/cm^3 [30]), and La_2O_3 (6.510 g/cm^3 [31]), respectively. Hardness and fracture toughness of each sample were measured using Shimadzu HV2 microhardness tester, after obtaining the mirror-like surface using 1 μm diamond paste. Compression strength of the samples was carried out using a universal testing machine (Devotrans FU 50kN, Turkey) under a loading rate of 2 mm min^{-1}. Three-point bending strength of the samples was determined using formula 2 at cross head speed of 1 mm/min until they are broken to the specimens with the dimensions 40 × 4 × 4 mm^3 prepared according to ASTM C1161-94 standard at 160 MPa [32]. The inner ring had a diameter of 10 mm, and the outer support ring had a diameter of 20 mm. The distance between inner spans was 20 mm. The sintered test bars were ground (1200 grit) on both sides before testing. Five specimens were tested for a single point.

$$\sigma_{\text{three-point bending}} = \frac{3PL}{2bh^2} \quad (2)$$

where *P* is the break load (N), *L* is the distance between inner spans (mm), *b* is the specimen width (mm), and *h* is the specimen thickness (mm).

Assessment of in vitro bioactivity

The specimens having the high mechanical properties were prepared in a disk shape with the dimensions of 11 × 4 mm^2 (diameter × thickness) after sanding up to 1200 mesh SiC paper and sterilization (autoclaving, 120 °C, 20 min) for in vitro tests. The assessment of in vitro bioactivity was carried out by soaking the pellets mounted vertically, in 40 mL SBF at pH 7.32 and maintained at 37 ± 1 °C, proposed by Kokubo et al. [33] for 3, 7, 15, and 30 days. The 40 mL SBF solutions used in the in vitro tests were changed every day. At a specified time, the samples were taken from the SBF solutions without damaging the apatite layers and cleaned using distilled water. Finally, the samples were dried at 60 °C for 12 h. The apatite layers on the surface of samples immersed in SBF solutions were investigated by SEM.

Results and discussion

The particle size distributions with SEM images of the starting materials (HA, Al_2O_3, La_2O_3) are given in Fig. 1. HA has an agglomerated particulates in irregular shapes and an average grain size of 7.096 μm. Al_2O_3

Table 1 Abbreviation and composition of the samples

Name	Sample codes	Composition (wt%)
Hydroxyapatite and alpha-alumina composites	HA	100% HA
	HA-5A	95% HA + 5%Al_2O_3
	HA-5A-0.5L	94.5% HA + 5% Al_2O_3 + 0.5% La_2O_3
	HA-5A-1.5L	93.5% HA + 5%Al_2O_3 + 1.5% La_2O_3
	HA-5A-2.5L	92.5% HA + 5%Al_2O_3 + 2.5% La_2O_3

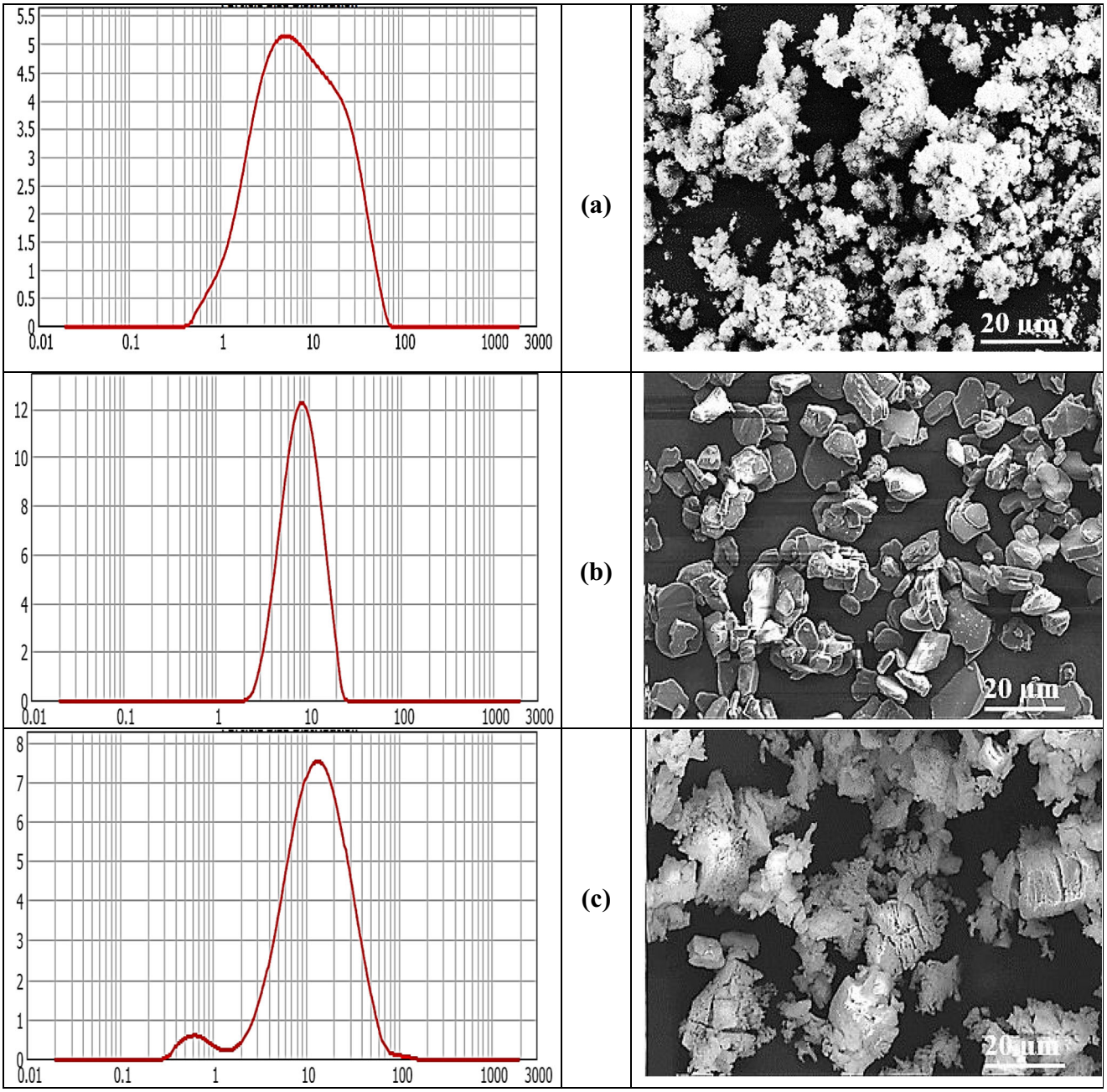


Fig. 1 The particle size distributions with SEM images of the raw materials **a** HA, **b** Al_2O_3, and **c** La_2O_3

presented an irregular shapes and an average grain size of 8.334 μm. La_2O_3 also possessed spongy shape and an average grain size of 12.578 μm. As shown in Table 2, HA can be used in biomedical applications because it agrees with ASTM F1185-88 standard [34].

Figure 2 shows the XRD patterns of HA without additives. HA slightly decomposed when there was no additives. When pure HA was sintered at 1100 °C, the HA phase partially transformed to β-TCP (JCPDS card number 98-007-6896), whereas for sintering at 1300 °C, it transformed to α-TCP (JCPDS card number 98-007-8499), and calcium oxide (CaO; JCPDS card number 98-003-4977) phases in addition to β-TCP. The intensity of β-TCP phase, which was detected at the 2θ position of 31.013°, increased by increasing temperature. The α-TCP and CaO phases were detected at the 2θ position of 30.699° and 37.401°. The presence of β-TCP and α-TCP may be due to the loss of OH^- in the structure when HA is heated in air at high temperature. The decomposition of HA without additives, when it was sintered at 1300 °C, can be explained by following reaction.

$$Ca_{10}(PO_4)_6(OH)_2 \rightarrow 3Ca_3(PO_4)_2 + CaO + H_2O \quad (3)$$

Table 2 Chemical composition of HA powder which was provided from Across Organics company Web site used as matrix material in the present study

Base elements	Type of impurity	ASTM F1185-88 (ppm)	HA (ppm)
Ca (39.894) P (18.498)	As		
	Hg	5	≤1
	Pb	30	≤5
	Cd	5	≤2
	Total of heavy metals	50	≤10
	Cl		≤1500
	Cu		≤20
	F		≤50
	Fe		≤400
	Mn		≤20
	SO_4^{2-}		≤5000

When the sintering temperature was increased from 1100 to 1300 °C, the stability of HA in HA-5A composite decreased at a high level compared to pure HA, as shown in Fig. 3. The sintered HA-5A composite contains several phases such as α-Al_2O_3, calcium aluminate phases, and TCP phases in addition to HA peaks. The characteristic peaks of α-Al_2O_3 (JCPDS card number 98-004-0109) at 2θ = 25.565°, 35.136°, 37.760°, and 43.335° were present in all the samples whereas the characteristics peak of $Ca_3Al_2O_6$ (JCPDS card number 98-008-9635) at 2θ = 33.210°, 40.975°, and 47.675° only detected for the sample, which was sintered at 1100 °C. The $Ca_3Al_2O_6$ is a calcium aluminate compound that occurs at low temperature (900–1100 °C) as a result of solid-state reaction between CaO and Al_2O_3 [35], as the following reaction.

$$3CaO + Al_2O_3 \rightarrow Ca_3Al_2O_6 \quad (4)$$

Diffraction patterns of $CaAl_4O_7$ phase (JCPDS card number 98-001-4312) were detected at 2θ = 25.468°, 28.966°, 32.492°, 34.550°, 35.443°, 41.309°, and 47.817°, when HA-5A sample was sintered at 1100 °C and 1200 °C. As stated by Gawalt et al. [36], it has the reactive groups for the attachment of organic acids to antibiotics, and it protects its existence up to 1200 °C in CaO-Al_2O_3 binary system [37], as the following reaction.

$$CaO + 2Al_2O_3 \rightarrow CaAl_4O_7 \quad (5)$$

$CaAl_2O_4$ phase (JCPDS card number 98-000-0144) was detected at 1200 °C and 1300 °C. The alumina increases the decomposition rate of HA to TCP at temperatures above 1150 °C [38], probably because of the formation of $CaAl_2O_4$ by the following reaction:

$$Ca_{10}(PO_4)_6(OH)_2 + Al_2O_3 \rightarrow 3Ca_3(PO_4)_2 + CaAl_2O_4 + H_2O \quad (6)$$

Solid-state reactions in ionic materials take place by the diffusion of ions across the interface. In the present case for the formation of aluminates, Ca^{2+} and Al^{3+} are the important species. There are two ways in which the reaction can take place. Al^{3+} can diffuse into the HA, or Ca^{2+} can diffuse from the HA into the alumina [39]. The formation of the abovementioned calcium aluminate phases in the HA-Al_2O_3 binary compositions is schematically illustrated in Fig. 4.

The solid solubility in Al_2O_3 is limited because of its close-packed structure; therefore, the formation of the aluminates probably takes place on the surface of the alumina particles. The removal of calcium must be compensated by the formation of oxygen vacancies, leading to a relaxation of the HA structure and monolithic HA is converted to calcium-deficient HA (Ca/P = 1.5) [39] as shown in Fig. 5.

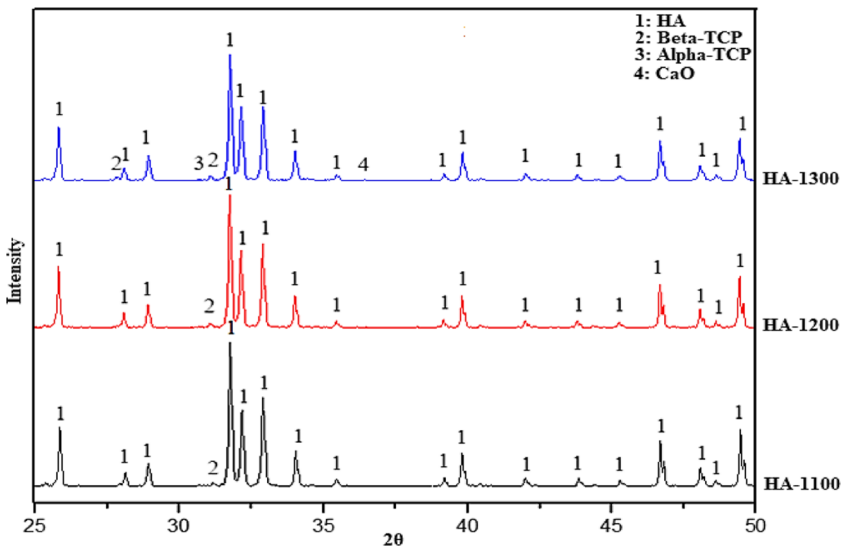


Fig. 2 XRD patterns of HA without additives

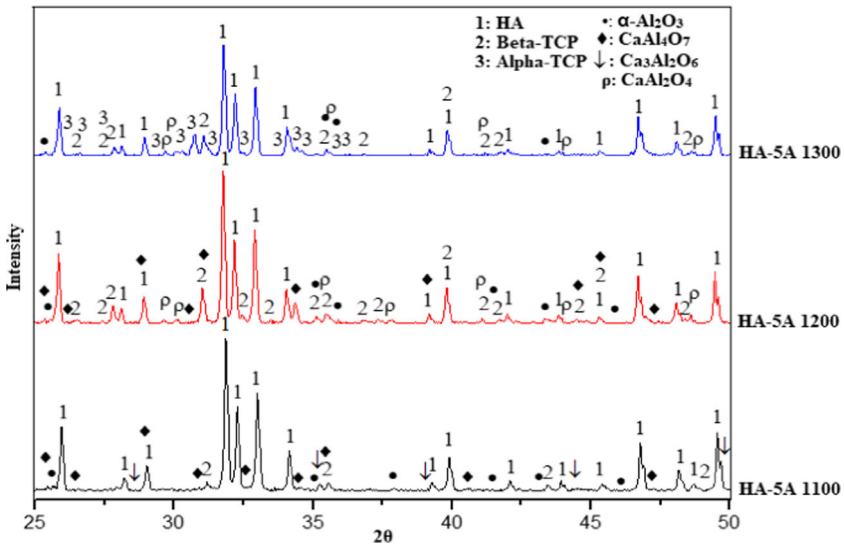


Fig. 3 XRD patterns of HA-5A composite

Figure 6 shows the XRD patterns of La_2O_3-added samples. The characteristic peaks of $Al_{11}La_{0.5}O_{17}$ (JCPDS card number 98-004-5273) and $CaAl_3LaO_7$ (JCPDS card number 98-003-0984) phases were detected at all La_2O_3-added composites. The formation of these phases can be explained by two main reasons: first is the similarity of distance between Ca-O (2.0 38 Å) [40], La-O (2.370 Å) [41], Al-O (1.97 Å) [42]; second is the similarity of ionic radii of Ca^{2+} (0.99 Å) [43], La^{3+} (1.016 Å) [44], and Al^{3+} (0.675 Å) [45]. No CaO phase was detected in any of HA sample with additives in the present study, although it had formed in previous studies about the composites of HA-Al_2O_3 [46] and HA-La_2O_3 [25] binary composites. It is related to two main reasons: first is the amount of additives in the present study was lower than the others; second is the presence of $CaAl_3LaO_7$ and $Al_{11}La_{0.5}O_{17}$ phases, which inhibit the solid-state reaction between Ca^{2+} and Al_2O_3 and the formation of free CaO, as shown in Fig. 7.

The percent fractions of HA and second phases were analyzed by Rietveld analysis (Table 3). It has been stated that HA

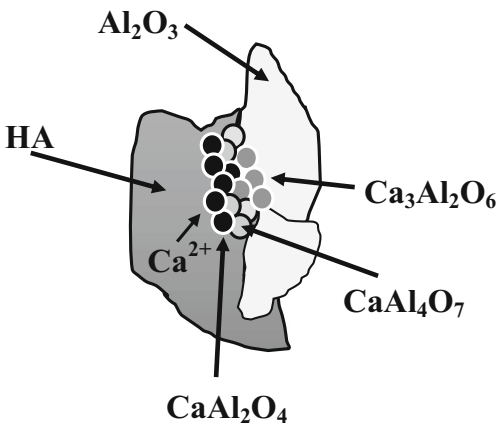


Fig. 4 Schematic representation of the formation of calcium aluminate phases in HA-Al2O3 binary composites

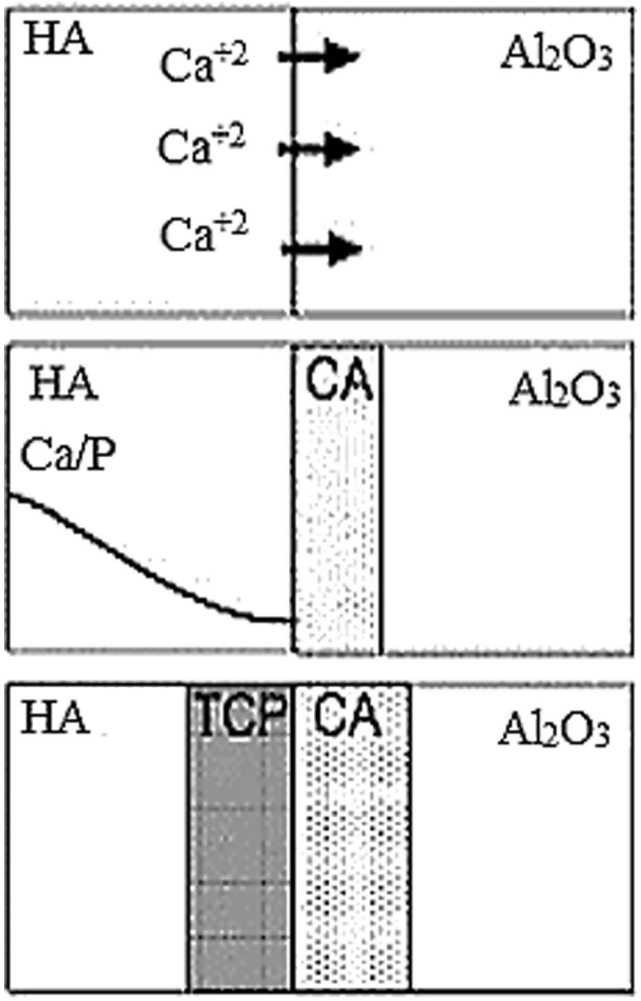


Fig. 5 Schematic representation the formation of TCP and calcium aluminate phases due to the solid-state reaction between HA and Al_2O_3 powders

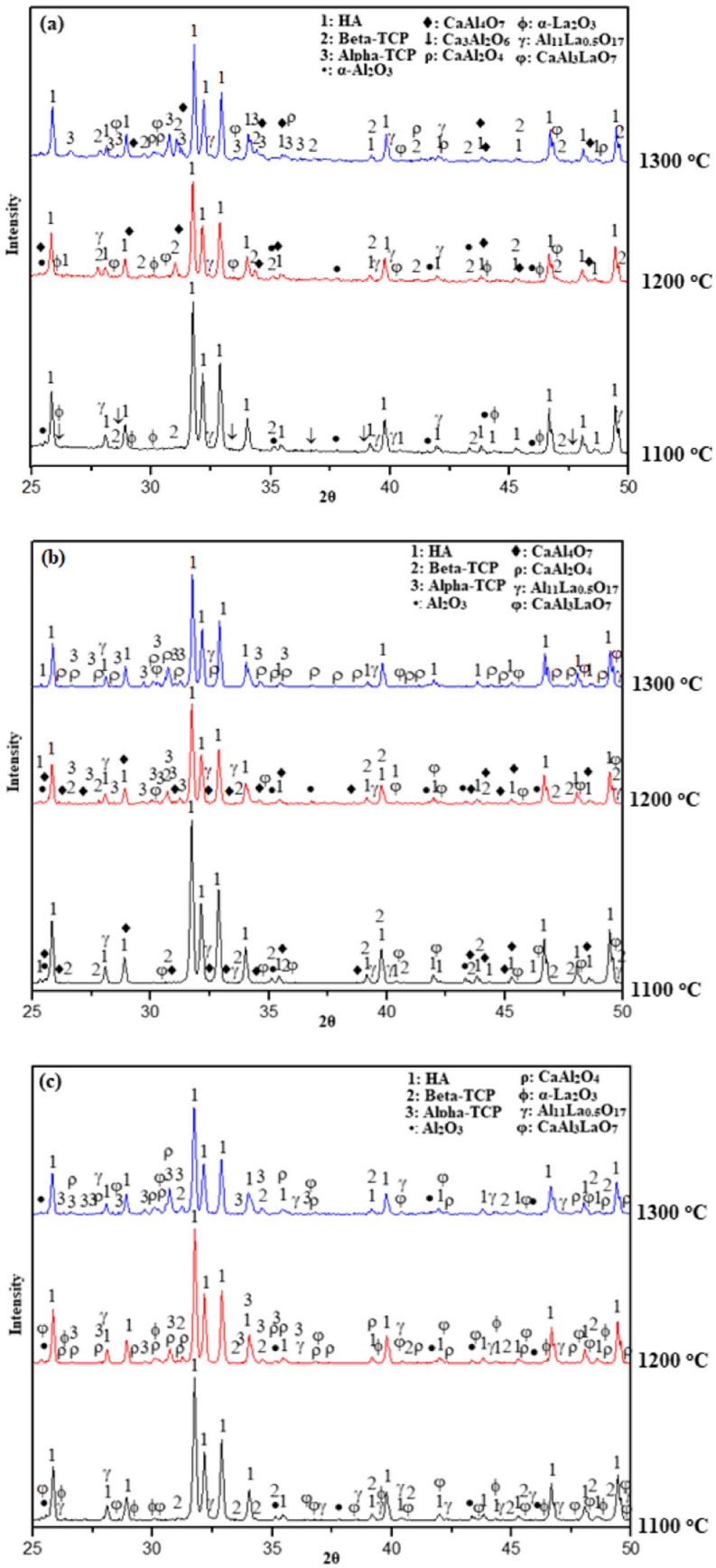


Fig. 6 The XRD patterns of **a** HA-5A-0.5L, **b** HA-5A-1.5L, and **c** HA-5A-2.5L composites

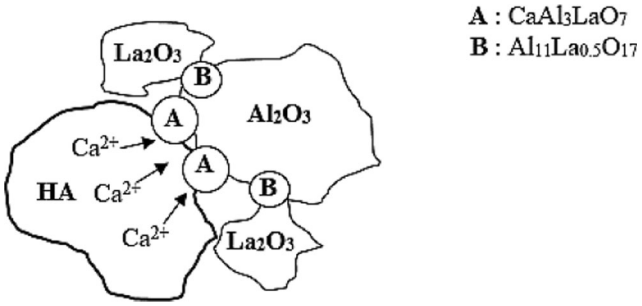


Fig. 7 Schematic view of the inhibition of the free CaO phase

without additives slightly decomposed at specified temperatures. The percent fractions of HA in HA-5A composite decreased from 94.7 to 72.6% by increasing temperature. The decomposition ratio of HA-5A composite is agreement with Evis [47]. Increasing the La_2O_3 ratio caused the formation of α-TCP phase at 1200 °C compared to pure HA and HA-5A composite. However, the addition of La_2O_3 into the HA-5A composite reduced the total decomposition ratio (β-TCP + α-TCP in HA), except HA-5A-2.5L composite at a negligible level, when it was sintered at 1300 °C. The decrease in total decomposition ratio for La_2O_3-added samples is related to the expansion of HA lattice structure and an increase in the crystal lattice energy and crystallinity of HA because of the coexistence of Ca^{2+} (0. 99 Å) and La^{3+} (1.0 16 Å) cations [48–50]. Moreover, the composite of La_2O_3-added HA-5A produced in the present study was more stable compared to HA-(5–20 wt%)ZrO_2-(0.5–2 wt%)YF_3 composite [51]. The total ratio of additive materials in the present study is lower than that of Usta et al. [51].

SEM micrographs of HA with and without additives sintered between 1100 and 1300 °C are presented in Fig. 8 and Fig. 9, respectively. Average grain sizes determined from the SEM images are given in Table 4. There was more grain growth on the surface of HA without additives after sintering at 1200 °C and 1300 °C, as shown in Table 4. It also included the microcracks, which was in the transgranular form.

The mechanical properties of HA with and without additives are shown in Fig. 10. It is seen that both composition and sintering temperature have striking effects on the mechanical strength. There were porosity up to 26.58 ± 0.89% for pure HA after sintering at 1100 °C, whereas it decreased to 2.91 ± 0.76% when the sintering temperature increased to 1300 °C. HA-5A composite without La_2O_3 additives exhibited the dense structure at 1100 °C, but sintering at elevated temperatures caused the more porosity compared to pure HA (2.91 ± 0.76% for pure HA, 3.04 ± 0.68% for HA-5A composite), and its density reached the maximum value of 2.99 ± 0.02 g/cm^3 with relative density of 94.05 ± 0.89%. However, the maximum density value of 2.97 ± 0.02 g/cm^3 with relative density of 92.83 ± 0.84% was obtained for HA-5A-L composites, when HA-5A reinforced with La_2O_3 at amount of 0.5 wt% after sintering at 1300 °C. Although the densification of HA without additives was generally more than composites, increasing the sintering temperature caused to decreasing the compressive strength from 130.20 ± 6.22 to 65.60 ± 5.59 MPa. Similarly, the decreasing of compressive strength for pure HA, between 1100 °C and 1300 °C, had also confirmed by Vallet-Regí et al. [52]. The increase in density of ceramic materials contributes to the improvement of mechanical properties; however, HA without additives, when it was sintered at temperatures of 1250–1300 °C, starts to decompose (transformation to secondary phases such as β and/or α-TCP, and CaO), which leads to reduction in mechanical properties [53–55]. The maximum compressive strength value of HA-5A composite (214 ± 32.50 MPa) was more than monolithic HA (130.20 ± 6.22 MPa). The maximum compressive strength of HA-5A is good agreement with Patel and Gohil [56]. However, the compressive strength of HA-5A composite decreased from 214 ± 32.50 to 149.7 ± 32.8 MPa when it was sintered at 1300 °C. Such a reduction could be attributed to the presence of α-TCP and $CaAl_2O_4$ phases into samples. As reported by Kim et al. [57], HA with the addition of α-Al_2O_3 resulted in the formation of $CaAl_2O_4$, which accelerated the decomposition of HA into the α-TCP phase. As in HA-5A composites, the maximum compressive strength values for La_2O_3-added samples were obtained at 1200 °C. The highest compressive strength was obtained to HA-5A composite added 0.5 wt% La_2O_3 as 230.50 ± 32.91 MPa. The highest compressive strength value obtained to HA-5A-0.5L composite is due to two main reasons:

Table 3 The percent fractions of HA and second phases

Sample	1100 °C			1200 °C			1300 °C		
	HA	β-TCP	α-TCP	HA	β-TCP	α-TCP	HA	β-TCP	α-TCP
HA	97.5	2.5	–	96.2	3.8	–	94.3	4.1	1.6
HA-5A	94.7	5.3	–	80.2	19.8	–	72.6	10.5	16.9
HA-5A-0.5L	99.3	0.7	–	89.4	10.6	–	78.0	9.5	12.5
HA-5A-1.5L	98.4	1.6	–	83.7	4.3	12.0	75.7	3.4	20.9
HA-5A-2.5L	97.1	2.9	–	82.7	3.7	13.6	72.5	5.0	23.5

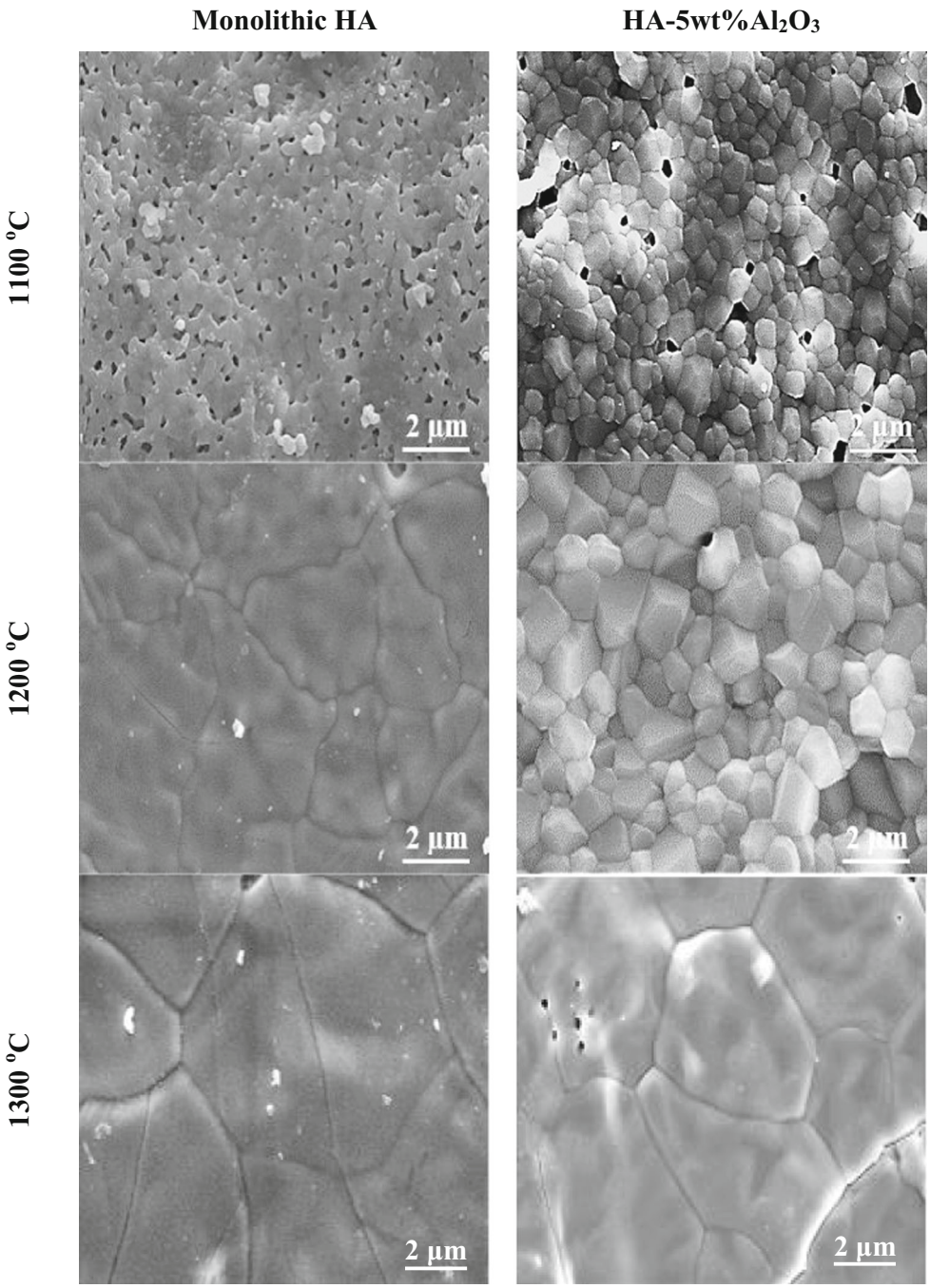


Fig. 8 The SEM images of monolithic HA and HA-5wt% Al_2O_3

1. Because the HA-5A-1.5L and HA-5A-2.5L composites have more porous structures than HA-5A-0.5L composite, their compressive strength values are lower than HA-5A-0.5L composite.
2. As the decomposition ratio of HA-5A-0.5L composite is lower than the HA-5A-1.5L, and HA-5A-2.5L composites, it has higher compressive strength than the others.

Increasing the sintering temperature from 1100 to 1300 °C and reducing the La_2O_3 content in the HA-5A-L composites led to decreasing the porosity from 29.45 to 3.34%. The higher porosity for higher La_2O_3 content is properly due to the mismatch between the different components leading to an inhibition of the sintering ability. The hardness of HA without additives attained to 4.87 ± 0.15 GPa by increasing temperature. The maximum hardness of the composites decrease by increasing porosity, and it reached 4.62 ± 0.48 GPa for HA-5A and 4.31 ± 0.28 GPa for HA-5A-L composites. The porosity and hardness were known to be inversely proportional; in other words, an increase in hardness requires a decrease in the porosity of the structure which is known as Duckworth–

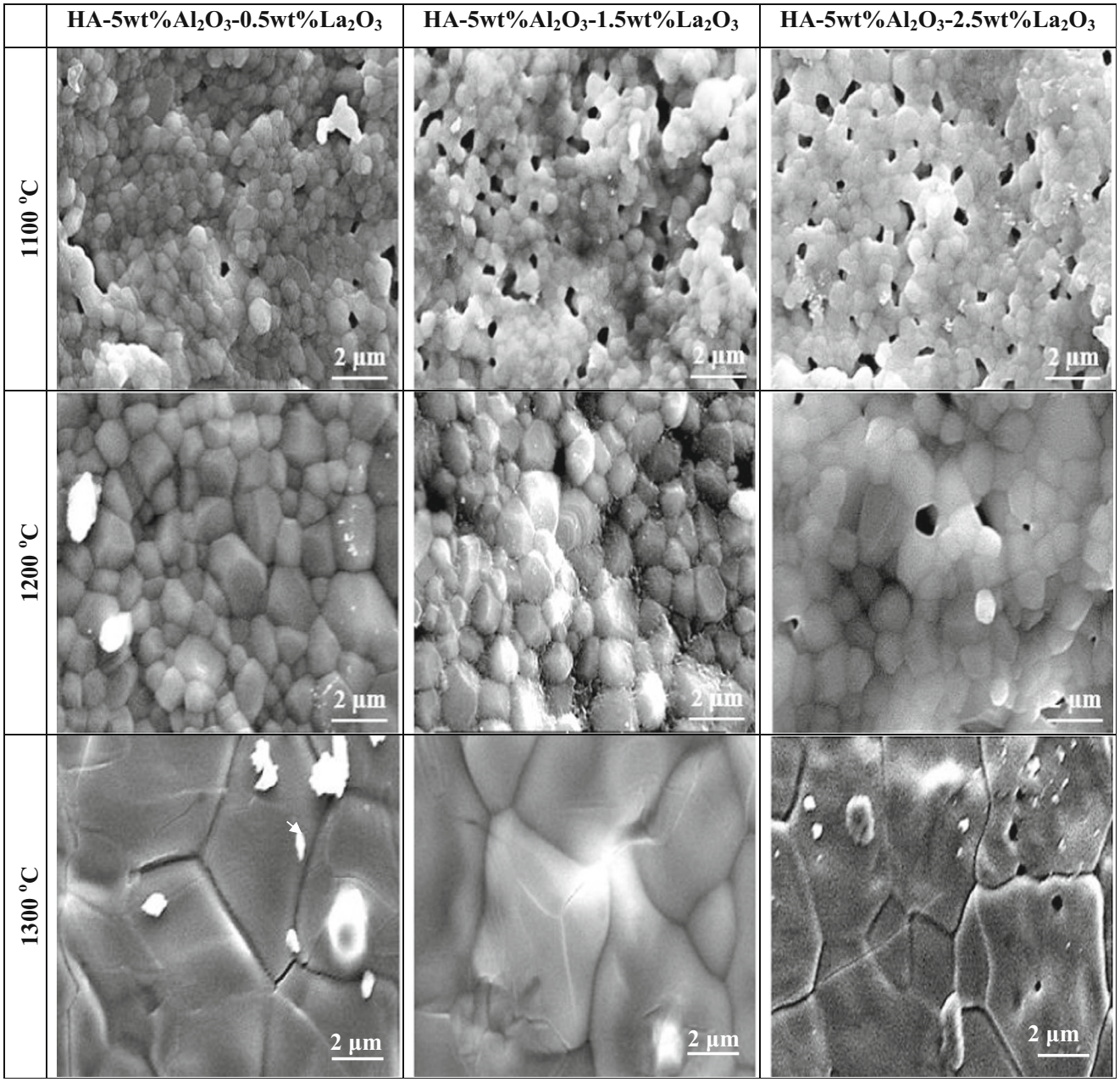


Fig. 9 SEM images of La_2O_3-added samples

Table 4 Average grain sizes of HA with and without additives measured from SEM images

Sample	Average grain size (µm)		
	1100 °C	1200 °C	1300 °C
HA	0.473 ± 0.035	7.955 ± 1.616	17.167 ± 2.156
HA-5A	0.427 ± 0.033	0.812 ± 0.110	10.171 ± 1.672
HA-5A-0.5L	0.352 ± 0.044	0.876 ± 0.061	8.890 ± 0.959
HA-5A-1.5L	0.334 ± 0.009	0.764 ± 0.109	7.100 ± 0.916
HA-5A-2.5L	0.313 ± 0.014	0.686 ± 0.164	6.676 ± 1.690

Knudsen model [26]. The highest fracture toughness value for pure HA increased with Al_2O_3 additive from 0.96 ± 0.05 to 1.95 ± 0.10 MPa $m^{1/2}$. The highest fracture toughness value of HA-A binary composite is in good agreement with Gautier et al. [58] (30 vol% Al_2O_3-HA, about 2.0 MPa $m^{1/2}$). It is seen from these values that the maximum fracture toughness value of 0.96 ± 0.05 MPa $m^{1/2}$ for pure HA can be increased at about two times by the addition of Al_2O_3 to HA. This is due to the fact that the calcium aluminate phases formed by the addition of Al_2O_3 resulted in the alteration and bridging of cracks occurring during the decomposition of HA, which strengthened the matrix against the formation of large cracks [59]. There are

two main reasons for the reduction in fracture toughness of pure HA: first is the decrease in the number of grains that will prevent the progress of cracks with increasing grain size; second is the formation of residual stresses in the sintered samples at elevated temperatures due to the decomposition of HA [60, 61]. A negligible increase was observed for the fracture toughness value of HA-5A-0.5L composite (1.99 ± 0.11 MPa $m^{1/2}$) compared to HA-5A composite (1.95 ± 0.10 MPa $m^{1/2}$). It may be explained the low elastic modulus of La_2O_3 compared with Al_2O_3. The increment in the fracture toughness of HA-5A composite by the addition of La_2O_3 at amount of 0.5 wt% was about 2.05%. While the three-point bending strength of pure HA decreased by increasing sintering temperature, the maximum three-point bending strength of monolithic HA was measured as 60.27 ± 9.93 MPa. The maximum three-point bending strength of monolithic HA obtained in the present study is compatible with the values of 57.4 MPa [62] and 69.5 MPa [63]. The three-point bending strength of the HA-5A composite presented the maximum value of 75.70 ± 2.40 MPa at the temperature of 1200 °C. However, the increase sintering temperature caused to decrease the three-point bending strength of HA-5A with and without La_2O_3 additive. The decreasing of three-point bending strength of HA-5A is due to the more decomposition ratios of the samples compared to 1200 °C, when they sintered at 1300 °C. Although sintering at 1300 °C caused to decrease the three-point bending strength of the samples, La_2O_3 additive HA-5A contributed to improvement of the three-point bending strength (from 75.70 ± 2.40 to 98.40 ± 7.49 MPa). Increasing the three-point bending strength of HA-5A by La_2O_3 additive is due to the inhibition of the grain growth of HA-5A composite. It is well known that a decrease in grain size increased the mechanical properties according to the Hall-Petch equation ($\sigma = \sigma_o + kd^{-1/2}$) [64].

The in vitro test was performed using SBF and observed under SEM. Figure 11 shows the surface morphologies of pure HA with and without additives. The apatite crystals on the surface of the samples started to form at the end of 3 days. The amount of apatite crystals, however, was higher than that

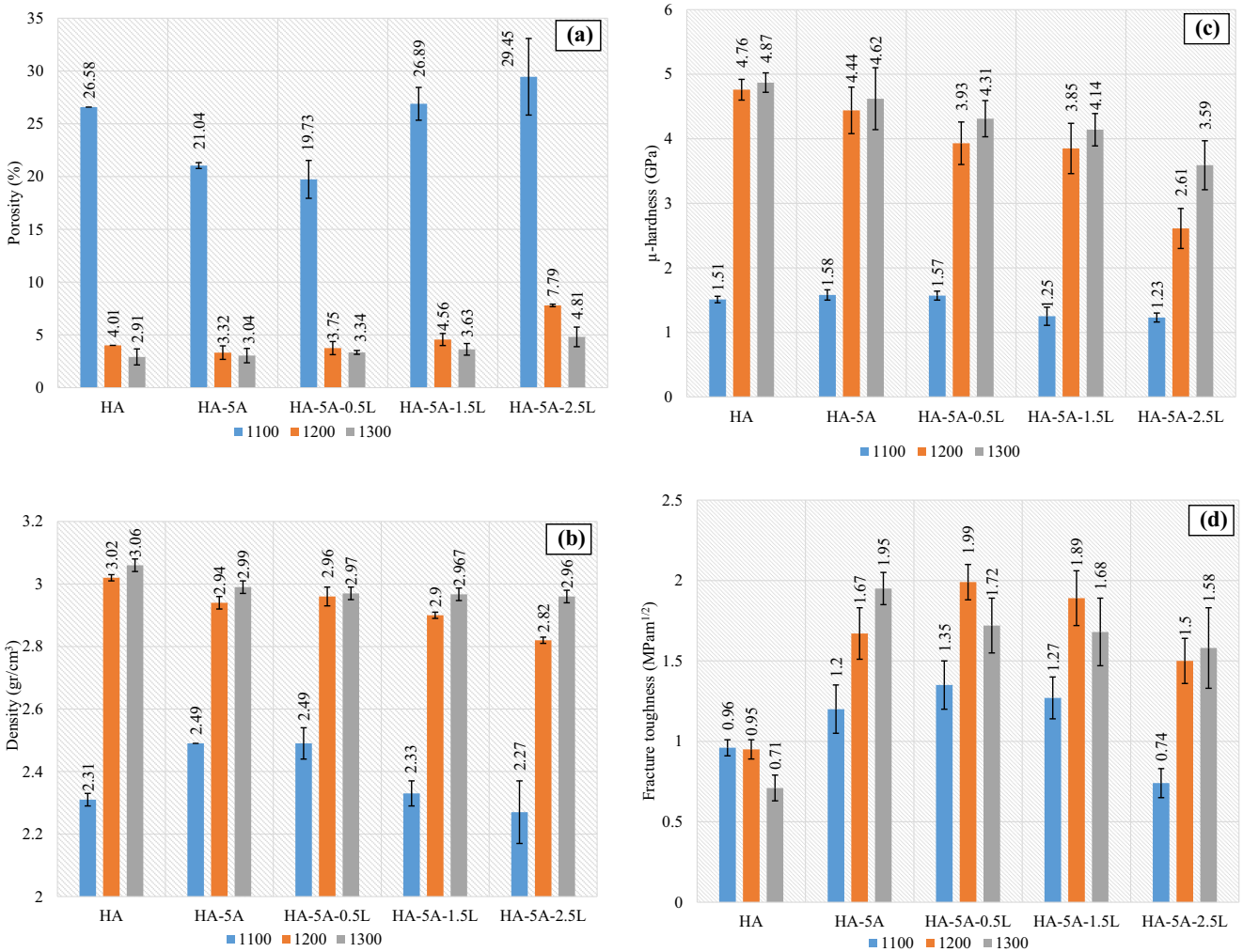


Fig. 10 The mechanical properties of HA with and without additives. **a** Porosity (%). **b** Density (g/cm^3). **c** μ-Hardness (GPa). **d** Fracture toughness (MPa $m^{1/2}$), **e** Three-point bending strength (MPa). **f** Compressive strength (MPa)

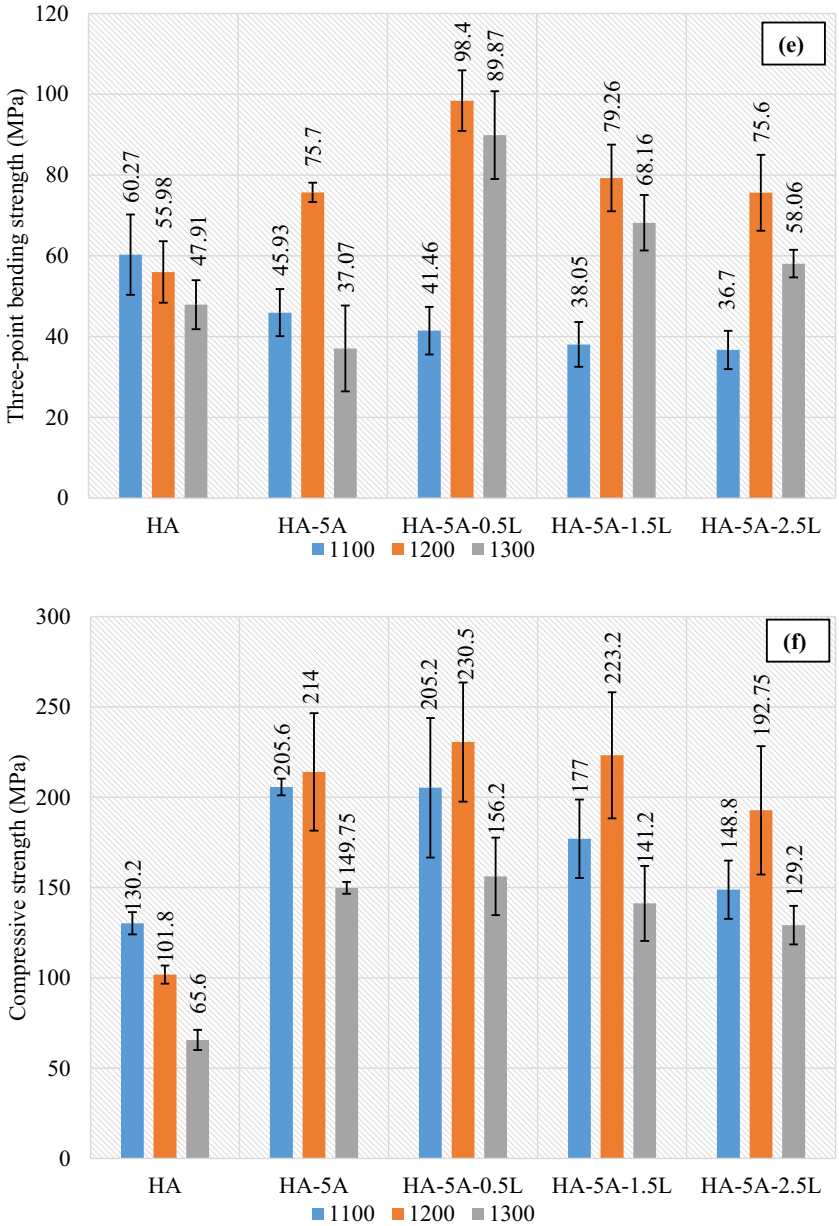


Fig. 10 (continued)

of the composites. After 7 days of immersing time, the apatite crystals began to grow in a dendritic form instead of a cubic shape for pure and La_2O_3-added HA. However, the apatite crystals continued to grow in cubic shapes for HA-5A composites. While the large part of the pure HA was covered by apatite layers after 15 days, the apatites on the surface of HA-5A and HA-5A-0.5L composite were thicker than that of pure HA. However, all of the surfaces of the sintered samples were covered by apatite layers after 30 days. It was determined that both morphologies and the amount of apatite layers deposited on the surface of the samples were dissimilar depending on the immersion time and compositions of the samples. The differences are due to the three main reasons: first is the porosity rates of the samples, second is the bioactivity properties of additive powders, and third is the types of the interphases that occurred during sintering. As reported by Chen et al. [65], the amount and proportion of the apatite layers formed on the surfaces of the samples increase by the porosity ratio increase. The porosity rates of the samples before the SBF testing were 26.58%, 3.32%, and 3.34% for pure HA, HA-5A, and HA-5A-0.5L, respectively. Although Al_2O_3 has higher mechanical properties compared to the HA, it is well known that Al_2O_3 is a bioinert ceramic, so the addition of Al_2O_3 to HA reduces the bioactivity property of HA. Therefore, the in vitro bioactivity of HA-5A composite was lower than that of pure HA and HA-5A-0.5L composite. In the other words, the addition of La_2O_3 contributed to the increase of bioactivity of the HA-5A composite.

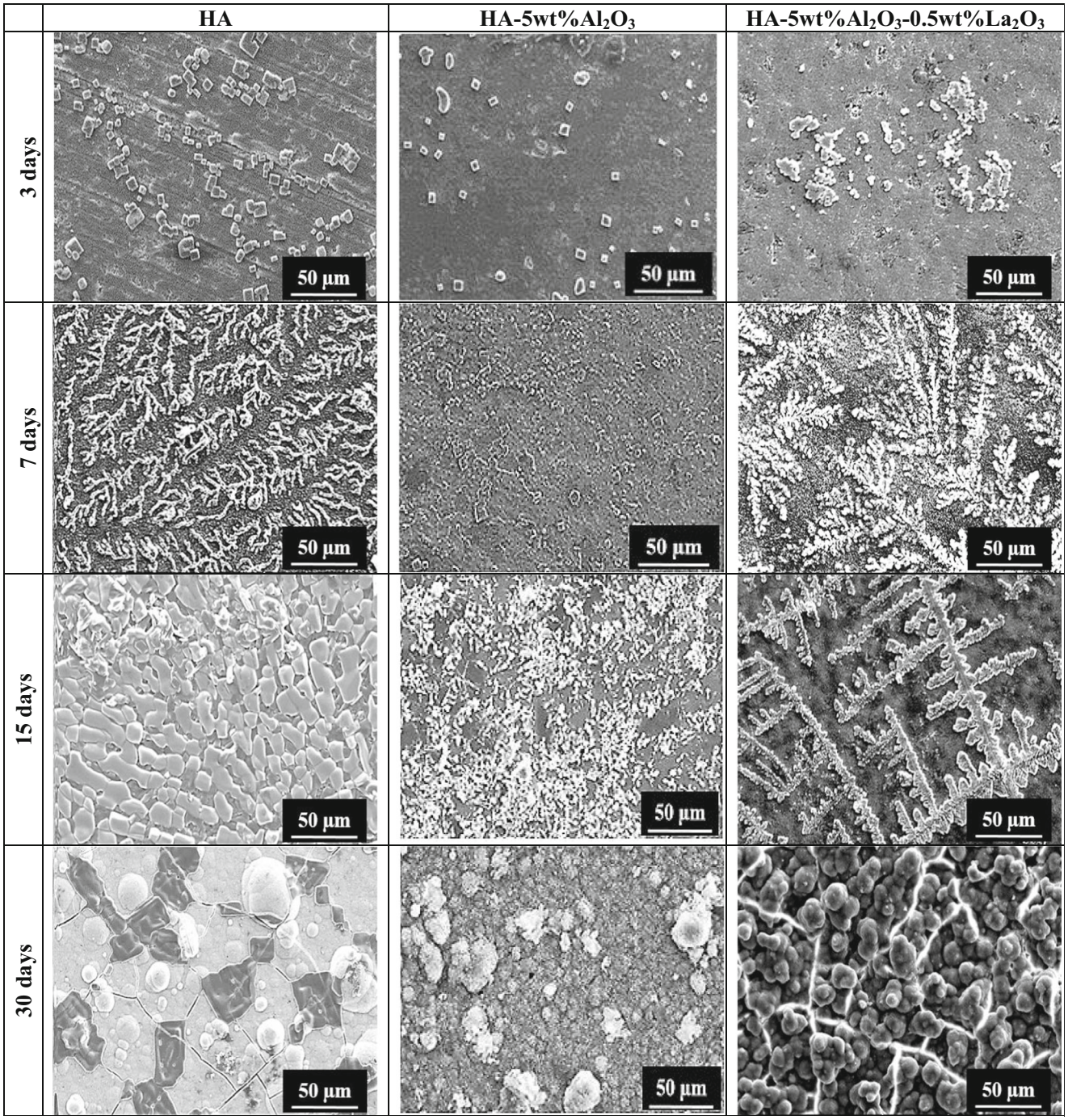


Fig. 11 The in vitro surface morphologies of HA with and without additives

Conclusions

The monolithic HA started to decomposition into secondary phases such as β- and/or α-TCP and CaO, when it was sintered at 1200 °C and 1300 °C, respectively. Moreover, the mechanical properties of monolithic HA decreased just before densification was completed. The highest mechanical strengths for pure HA were obtained at sintering temperature of 1100 °C. Al_2O_3 addition led to increment in the decomposition ratio of HA. While the decomposition ratio is less than 5% for pure HA, it attained to 31.8% for HA-5A composites, respectively. Growth of HA grains was inhibited by the addition of Al_2O_3 and La_2O_3. For this reason, all mechanical properties of pure HA, except hardness and densification, was improved higher than the rate of 60%. Although the addition of Al_2O_3 leads to reduction of the in vitro bioactivity of HA, the addition of La_2O_3 contributed to improvement of its bioactivity.

Funding The authors thank the economic support of Scientific Research Centre of Marmara University (Project No. FEN-K-150218-0051).

References

1. Prakasam, M., Locs, J., Salma-Ancane, K., Loca, D., Largeteau, A., Berzina-Cimdina, L.: Fabrication, properties and applications of dense hydroxyapatite: a review. J. Funct. Biomater. **6**, 1099–1140 (2015)
2. Ghazanfari, S.M.H., Zamanian, A.: Phase transformation, microstructural and mechanical properties of hydroxyapatite/alumina nanocomposite scaffolds produced by freeze casting. Ceram. Int. **39**, 9835–9844 (2013)
3. Champion, E., Gautier, S., Bernache-Assollant, D.: Characterization of hot pressed Al_2O_3-platelet reinforced hydroxyapatite composites. J. Mater. Sci. Mater. Med. **7**, 125–130 (1996)
4. Brzezińska-Miecznik, J., Haberko, K., Sitarz, M., Bućko, M.M., Macherzyńska, B., Lach, R.: Natural and synthetic hydroxyapatite/zirconia composites: a comparative study. Ceram. Int. **42**, 11126–11135 (2016)
5. Lih-Jyh, F., Ya-Jing, H., Wen-Cheng, C., Dan-Jae, L.: Preparation of micro-porous bioceramic containing silicon-substituted hydroxyapatite and beta-tricalcium phosphate. Mater. Sci. Eng. C. **75**, 798–806 (2017)
6. Hannora, A.E., Ataya, S.: Structure and compression strength of hydroxyapatite/titania nanocomposites formed by high energy ball milling. J. Alloys Compd. **658**, 222–233 (2016)
7. Bozkurt, Y., Gokce, H., Pazarlioglu, S., Salman, S.: The effect of yttrium oxide reinforcement on the microstructural and mechanical properties of biologically derived hydroxyapatite. Acta Phys. Pol. A. **127**(4), 1403–1406 (2015)
8. Bartonickova, E., Vojtisek, J., Tkacz, J., Porizka, J., Masilko, J., Moncekova, M., Parizek, L.: Porous Ha/alumina composites intended for bone-tissue engineering. Mater. Technol. **51**(4), 631–636 (2017)
9. Aminzare, M., Eskandari, A., Baroonian, M.H., Berenov, A., Hesabi, Z.R., Taheri, M., Sadrnezhaad, S.K.: Hydroxyapatite nanocomposites: synthesis, sintering and mechanical properties. Ceram. Int. **39**, 2197–2206 (2013)
10. Afzal, M.A.F., Kesarwani, P., Reddy, K.M., Kalmodia, S., Basu, B., Balani, K.: Functionally graded hydroxyapatite-alumina-zirconia biocomposite: synergy of toughness and biocompatibility. Mater. Sci. Eng. C. **32**, 1164–1173 (2012)
11. Li, J., Fartash, B., Herrnansson, L.: Hydroxyapatite-alumina composites and bone-bonding. Biomater. **16**, 417–422 (1995)
12. Sivaperumal, V.R., Mani, R., Nachiappan, M.S., Arumugam, K.: Direct hydrothermal synthesis of hydroxyapatite/alumina nanocomposite. Mater. Charact. **134**, 416–421 (2017)
13. Tayebi, S., Mirjalili, F., Samadi, H., Nemati, A.: The effect of additives on the properties of HAp-Al_2O_3 nano-composite powders. J. Ceram. Process. Res. **17**(10), 1033–1041 (2016)
14. Evis, Z., Doremus, R.H.: Effect of AlF_3, CaF_2 and MgF_2 on hot-pressed hydroxyapatite-nanophase alpha-alumina composites. Mater. Res. Bull. **43**, 2643–2651 (2008)
15. Sung-Jin, K., Hee-Gon, B., Jun-Ho, S., Sang-Yeup, P.: Effect of fluoride additive on the mechanical properties of hydroxyapatite/alumina composites. Ceram. Int. **35**, 1647–1650 (2009)
16. Hae-Won, K., Young-Hag, K., Seung-Beom, S., Hyoun-Ee, K.: Properties of fluoridated hydroxyapatite-alumina biological composites densified with addition of CaF_2. Mater. Sci. Eng. C. **23**, 515–521 (2003)
17. Bulut, B., Erkmen, Z.E., Kayali, E.S.: Biocompatibility of hydroxyapatite-alumina and hydroxyapatite-zirconia composites including commercial inert glass (CIG) as a ternary component. J. Ceram. Sci. Tech. **07**(03), 263–276 (2016)
18. Kalkandelen, C., Gunduz, O., Akan, A., Oktar, F.N.: Part 1: clinoptilolite-alumina-hydroxyapatite composites for biomedical engineering. J. Aust. Ceram. Soc. **53**, 91–99 (2017)
19. Li-Li, W., Xiu-Feng, W., Xu, D., Hong-Tao, J.: Preparation of HA-bioglass-Al_2O_3 biological composite. Mater. Manuf. Process. **28**, 980–983 (2013)
20. Yelten, A., Yilmaz, S., Oktar, F.N.: Sol-gel derived alumina-hydroxyapatite-tricalcium phosphate porous composite powders. Ceram. Int. **38**, 2659–2665 (2012)
21. Guidara, A., Chaari, K., Bouaziz, J.: Effect of titania additive on structural and mechanical properties of alumina-fluorapatite composites. J. Mater. Sci. Technol. **28**(12), 1130–1136 (2012)
22. Branda, F., Arcobello-Varlese, F., Costantini, A., Luciani, G.: Effect of the substitution of M_2O_3 (M=La, Y, In, Ga, Al) for CaO on the bioactivity of $2.5CaO.2SiO_2$ glass. Biomater. **23**, 711–716 (2002)
23. Shin-Ike, M., Tsutsui, J., Tanaka, A., Murayama, S., Fujita, A.: Attempts to improve the strength of sintered lanthanum-containing hydroxyapatites. J. Osaka Dent. Uni. **52**, 854–861 (1989)
24. Tanaka, A., Nishimura, Y., Sakaki, T., Fujita, A., Shin-Ike, T.: Histologic evaluation of tissue response to sintered lanthanum-containing hydroxyapatites subcutaneously implanted in rats. J. Osaka Dent. Uni. **23**, 111–116 (1989)
25. Bozkurt, Y., Pazarlioglu, S., Gokce, H., Gurler, I., Salman, S.: Hydroxyapatite lanthanum oxide composites. Acta Phys. Pol. A. **127**(4), 1407–1409 (2015)
26. Khoshsima, S., Yilmaz, B., Tezcaner, A., Evis, Z.: Structural, mechanical and biological properties of hydroxyapatite-zirconia-lanthanum oxide composites. Ceram. Int. **42**, 15773–15779 (2016)
27. Khoshsima, S., Alshemary, A.Z., Tezcaner, A., Surdem, S., Evis, Z.: Impact of B_2O_3 and La_2O_3 addition on structural, mechanical and biological properties of hydroxyapatite. Process. Appl. Ceram. **12**(2), 143–152 (2018)
28. Sato, K., Yugami, H., Hashida, T.: Effect of rare-earth oxides on fracture properties of ceria ceramics. J. Mater. Sci. **39**, 5765–5770 (2004)
29. Majling, J., Znáik, P., Palová, A., Stevīk, S., Kovalīk, S., Agrawal, D.K., Roy, R.: Sintering of the ultrahigh pressure densified hydroxyapatite monolithic xerogels. J. Mater. Res. **12**(1), 198–202 (1997)
30. Rahimiana, M., Ehsani, N., Parvin, N., reza Baharvandi, H.: The effect of particle size, sintering temperature and sintering time on the properties of Al-Al_2O_3 composites, made by powder metallurgy. J. Mater. Process. Technol. **209**, 5387–5393 (2009)
31. Kwon, J., Dai, M., Halls, M.D., Langereis, E., Chabal, Y.J., Gordon, R.G.: In situ infrared characterization during atomic layer deposition of lanthanum oxide. J. Phys. Chem. C. **113**, 654–660 (2009)
32. ASTM C1161-94 (1996) Standard test method for flexural strength of advanced ceramics at ambient temperature. Annual Book of ASTM Standards, USA
33. Kokubo, T., Yamamuro, T., Hench, L.L., Wilson, J.: Handbook on bioactive ceramics: bioactive glasses and glass-ceramics, vol. 1. CRC Press, Boca Raton (1990)
34. ASTM F 1185-88 (1993) Standard specification for composition of ceramic hydroxylapatite for surgical implants. American Society for Testing and Materials, 2000, West Conshohocken, PA, USA
35. Steele, F.A., Davey, W.P.: The crystal structure of tricalcium aluminate. J. Am. Chem. Soc. **51**(8), 2283–2293 (1975)
36. Palchesko, R.N., McGowan, K.A., Gawalt, E.S.: Surface immobilization of active vancomycin on calcium aluminum oxide. Mater. Sci. Eng. C. **31**, 637–642 (2011)

37. Tas, C.A.: Chemical preparation of the binary compounds in the calcia-alumina system by self-propagating combustion synthesis. J. Am. Ceram. Soc. **81**(11), 2853–2863 (1998)
38. Evis, Z., Doremus, R.H.: A study of phase stability and mechanical properties of hydroxylapatite-nanosize α-alumina composites. Mater. Sci. Eng. C. **27**, 421–425 (2007)
39. Viswanath, B., Ravishankar, N.: Interfacial reactions in hydroxyapatite/alumina nanocomposites. Scr. Mater. **55**, 863–866 (2006)
40. Ueda, J., Shinoda, T., Tanabe, S.: Evidence of three different Eu^{2+} sites and their luminescence quenching processes in $CaAl_2O_4$:Eu^{2+}. Opt. Mater. **41**, 84–89 (2015)
41. Kazin, P.E., Pogosova, M.A., Trusov, L.A., Kolesnik, I.V., Magdysyuk, O.V., Dinnebier, R.E.: Crystal structure details of La- and Bi-substituted hydroxyapatites: evidence for LaO^+ and BiO^+ with a very short metal-oxygen bond. J. Solid State Chem. **237**, 349–357 (2016)
42. Choi, M., Janotti, A., Van de Walle, C.G.: Native point defects and dangling bonds in α-Al_2O_3. J. Appl. Phys. **113**, 044501 (2013)
43. Krishna, R.H., Nagabhushana, B.M., Nagabhushana, H., Chakradhar, R.P.S., Murthy, N.S., Sivaramakrishna, R., Shivakumara, C., Rao, J.L., Thomas, T.: Combustion synthesis approach for spectral tuning of Eu doped $CaAl_2O_4$ phosphors. J. Alloys Compd. **589**, 596–603 (2014)
44. Mansour, S.F., Hemeda, O.M., El-Dek, S.I., Salem, B.I.: Influence of La doping and synthesis method on the properties of $CoFe_2O_4$ nanocrystals. J. Magn. Magn. Mater. **420**, 7–18 (2016)
45. Cerrillo, J.G., Mendoza, A.N.C., Romero, P.M.M., Granadosa, A.H., Hu, H.: Improvement of the morphological and electrical characteristics of Al^{3+}, Fe^{3+} and Bi^{3+}-doped TiO_2 compact thin films and their incorporation into hybrid solar cells. Mater. Sci. Semicond. Process. **72**, 106–114 (2017)
46. Chiba, A., Kimura, S., Raghukandan, K., Morizono, Y.: Effect of alumina addition on hydroxyapatite biocomposites fabricated by underwater-shock compaction. Mater. Sci. Eng. A. **350**, 179–183 (2003)
47. Evis, Z.: Al^{3+} doped nano-hydroxyapatites and their sintering characteristics. J. Ceram. Soc. Jpn. **114**, 1001–1004 (2006)
48. Guo, D.G., Wang, A.H., Han, Y., Xu, K.W.: Characterization, physicochemical properties and biocompatibility of La-incorporated apatites. Acta Biomater. **5**, 3512–3523 (2009)
49. Yang, H., Zhang, L., Xu, K.W.: Effect of fabrication processes on orientation growth of La/HAP crystal. J. Mater. Process. Technol. **207**, 276–282 (2008)
50. Lou, W., Dong, Y., Zhang, H., Jin, Y., Hu, X., Ma, J., Liu, J., Wu, G.: Preparation and characterization of lanthanum-incorporated hydroxyapatite coatings on titanium substrates. Int. J. Mol. Sci. **16**, 21070–21086 (2015)
51. Aykul, A., Kutbay, I., Evis, Z., Usta, M.: Effect of YF_3 on the phase stability and sinterability of hydroxyapatite-partially stabilized zirconia composites. Ceram. Int. **39**, 7869–7877 (2013)
52. Rodríguez-Lorenzo, L.M., Vallet-Regí, M., Ferreira, J.M.F.: Fabrication of hydroxyapatite bodies by uniaxial pressing from a precipitated powder. Biomater. **22**, 583–588 (2001)
53. Gu, Y.W., Loh, N.H., Khor, K.A., Tor, S.B., Cheang, P.: Spark plasma sintering of hydroxyapatite powders. Biomater. **23**, 37–43 (2002)
54. Khalil, K.A., Kim, S.W., Kim, H.Y.: Consolidation and mechanical properties of nanostructured hydroxyapatite-(ZrO_2+3mol%Y_2O_3) bioceramics by high-frequency induction heat sintering. Mater. Sci. Eng. A. **456**, 368–372 (2007)
55. Gu, Y.W., Khor, K.A., Cheang, P.: Bone-like apatite layer formation on hydroxyapatite prepared by spark plasma sintering (SPS). Biomater. **25**, 4127–4134 (2004)
56. Patel, N.R., Gohil, P.P.: A review on biomaterials: scope, applications & human anatomy significance. Int. J. Emerging Technol. Adv. Eng. **2**(4), 91–101 (2012)
57. Kim, H.W., Noh, Y.J., Koh, Y.H., Kim, H.E.: Enhanced performance of flourine substituted hydroxyapatite composites for hard tissue engineering. J. Mater. Sci. Mater. Med. **14**, 899–904 (2003)
58. Gautier, S., Champion, E., Bernache-Assollant, D.: Toughening characterization in alumina platelets-hydroxyapatite matrix composites. J. Mater. Sci. Mater. Med. **10**, 533–540 (1999)
59. Kim, S., Kong, Y.M., Lee, I.S., Kim, H.E.: Effect of calcinations of starting powder on mechanical properties of hydroxyapatite-alumina bioceramic composite. J. Mater. Sci. Mater. Med. **13**, 307–310 (2002)
60. Thangamani, N., Chinnakali, K., Gnanam, F.D.: The effect of powder processing on densification, microstructure and mechanical properties of hydroxyapatite. Ceram. Int. **28**, 355–362 (2002)
61. Kobayashi, S., Kawai, W., Wakayama, S.: The effect of pressure during sintering on the strength and the fracture toughness of hydroxyapatite ceramics. J. Mater. Sci. Mater. Med. **17**, 1089–1093 (2006)
62. Kothapalli, C., Wei, M., Vasiliev, A., Shaw, M.T.: Influence of temperature and concentration on the sintering behavior and mechanical properties of hydroxyapatite. Acta Mater. **52**, 5655–5663 (2004)
63. Zhang, J., Maeda, M., Kotobuki, N., Hirose, M., Ohgushi, H., Jiang, D., Iwasa, M.: Aqueous processing of hydroxyapatite. Mater. Chem. Phys. **99**, 398–404 (2006)
64. Seo, D.S., Lee, J.K.: Dissolution-resistance of glass-added hydroxyapatite composites. Met. Mater. Int. **15**(2), 265–271 (2009)
65. Chen, Q.Z., Rezwan, K., Armitage, D., Nazhat, S.N., Boccaccini, A.R.: The surface functionalization of 45S5 bioglass-based glass-ceramic scaffolds and its impact on bioactivity. J. Mater. Sci. Mater. Med. **17**, 979–987 (2006)

Publisher's note Springer Nature remains neutral with regard to jurisdictional claims in published maps and institutional affiliations.